Fixed-Step Friction Simulation: From Classical Coulomb Model To Modern Continuous Models

Ryo Kikuuwe, Naoyuki Takesue, Akihito Sano, Hiromi Mochiyama, and Hideo Fujimoto
Touch Tech Lab Funded By Toyota, Nagoya Institute of Technology, Nagoya, Aichi 466-8555, Japan
kikuuwe@ieee.org

***Abstract*— Friction force is cumbersome in numerical simulations due to its discontinuity at zero velocity. Fixed-step simulation techniques are especially desirable for control purposes, such as haptic friction rendering and friction compensation. Previous techniques have difficulties especially in numerical robustness and extensibility to multidimensional cases. This paper proposes two discrete-time friction models that can be used in fixed-step simulations. They can be used in multidimensional space, and can capture arbitrary velocity-dependent friction phenomena. The first one is a discrete-time discontinuous model. This model determines the friction force so that the velocity reaches zero in finite time by using the values of the mass and the timestep size. The second one is a discrete-time continuous model, which is a serial coupling of the discontinuous model and a linear viscoelastic element. This model is useful for haptic rendering because it is formulated as a velocity-input, force-output system. The second model can be extended into a more sophisticated friction model, which exhibits a hysteresis behavior in the presliding regime. Results of numerical simulations and an experiment are presented.**

I. Introduction

Friction exists in all mechanical systems and everything in our everyday lives. Modeling of friction is important for simulation of mechanical systems, for model-based control, and for displaying realistic sense of touch through a haptic device. Friction force is highly nonlinear especially at very low velocity. This gives rise to difficulty in fixed-step numerical simulation of friction phenomena for the purposes of control and haptic rendering.

Numerous models of friction force have been proposed by researchers [1], [2]. These models can be mainly classified into two types: the discontinuous type and the continuous type. In discontinuous models, the friction force is discontinuous at zero velocity, and when the velocity is zero (i.e., in the sticking regime), the friction force acts to balance the other forces to maintain zero velocity. Continuous models consider small elastic displacement (presliding displacement) in the sticking regime [3]–[6]. Modeling of nonlinearity and hysteresis in the presliding displacement is attracting interest.

An advantage of discontinuous models is their intuitive simplicity. However, these models are mathematically cumbersome because their definition at zero velocity and that at a nonzero velocity are completely different. One approach is to use the threshold velocity as the boundary between zero and nonzero velocity regions [7], [8]. However, the selection of the threshold strongly influences the behaviors of models [9], and an inappropriate threshold causes energy-generating friction forces. Another approach is to use a finite state machine based on the detection of zero-velocity crossings (i.e., velocity reversals) [10]. This approach, however, is difficult to be applied to multidimensional cases [11] because velocity reversals cannot be defined strictly in multidimensional space. Adaptive timestep approaches for accurate zero-crossing detections are not suitable for realtime computation for control purposes.

Continuous models are more accurate than discontinuous models provided that various parameters regarding microscopic dynamics of the surfaces are adequately given. The equations defining these models are difficult to interpret physically because they are based on empirical data. One of their advantages is that they are mathematically convenient because they are formulated as a velocity-input, force-output system.

This paper presents discrete-time representations of discontinuous and continuous friction models for the purpose of fixed-step simulations. First, we present a new discrete-time discontinuous model. This model determines the friction force so that the velocity reaches exactly zero in finite time by using the values of the mass and the timestep size. This friction force is always dissipative. This model does not include arbitrariness of the threshold setting, and it is easily extended into multidimensional cases. Moreover, it can easily include velocity-dependent friction phenomena, such as Stribeck and viscous effects. Next, we present a discrete-time continuous friction model, which is a serial coupling of the discontinuous friction model and a linear viscoelastic element. This model can be further expanded into a more sophisticated continuous friction model, which exhibits a realistic hysteresis behavior in the presliding regime.

In the rest of this paper, we start from a brief review on previous friction models in section II. Next, we propose a new discrete-time discontinuous friction model in section III. Further, in section IV, we expand this model into continuous models. We perform 4 sets of simulations in section V and an experiment of haptic friction rendering in section VI. Section VII provides the conclusion.

II. Previous Models of Friction

A. Discontinuous Models

Assume that a rigid object is in contact with a fixed surface and moving at a velocity v with respect to the surface, as shown in Fig. 1(a). The equation of motion of the object is described as

$$M\dot{v} = h + f, \tag{1}$$

where M is the mass of the object, f is the friction force, and h is the gross force acting on the object from all other sources.

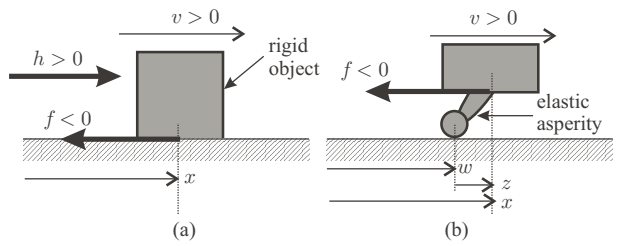

Fig. 1. Schematic representations of friction models. (a) a discontinuous model, and (b) a continuous model.

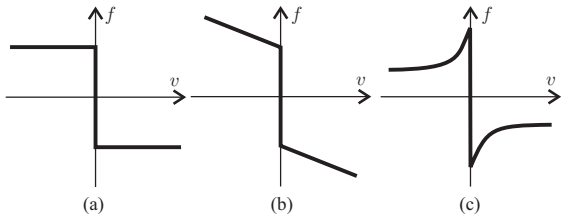

Fig. 2. Force-velocity relations in discontinuous friction models: (a) the Coulomb friction force, (b) Coulomb plus viscous friction force, and (c) Coulomb friction force plus Stribeck effect.

In discontinuous friction models, the friction force, f, is generally described as $f = \Phi(v, h)$ where

$$\Phi(v,h) = \begin{cases} -h & \text{if } v = 0 \wedge |h| \le |\phi(\pm 0)| \\ -\mathrm{sgn}(h)|\phi(\pm 0)| & \text{if } v = 0 \wedge |h| > |\phi(\pm 0)| \\ \phi(v) & \text{otherwise.} \end{cases} \quad (2)$$

Here, $\phi(v)$ is a function that satisfies $\phi(v)v \le 0$ for all $v \neq 0$ and has limits as $v \to +0$ and $v \to -0$. For simplicity of further discussion, we assume $\lim_{v\to -0} \phi(v) = -\lim_{v\to +0} \phi(v)$. Hereafter, we write $|\phi(\pm 0)| = \lim_{v\to -0} \phi(v)$.

The simplest friction model is the Coulomb friction model, which is illustrated in Fig. 2(a). Its representation can be obtained by specializing (2) by

$$\phi(v) = -\mathrm{sgn}(v)F, \quad (3)$$

where $F > 0$ is called the kinetic friction force. In general, the friction force depends on the velocity due to the surface mechanics and the lubricants between the two surfaces. Fig. 2(b) depicts the case when the viscous friction is present, and Fig. 2(c) depicts the so-called Stribeck effect [1], [2].

In usual dry friction, the maximum static friction force is larger than the kinetic friction force, namely,

$$f = \begin{cases} -h & \text{if } v = 0 \wedge |h| \le F_S \\ -\mathrm{sgn}(h)F_S & \text{if } v = 0 \wedge |h| > F_S \\ \phi(v) & \text{otherwise,} \end{cases} \quad (4)$$

where $F_S > |\phi(\pm 0)|$. This representation is mathematically troublesome though it is more general than (2). In stead of this, we can use steep Stribeck curves (shown in Fig. 2(c)) to represent the large friction force in the neighborhood of zero velocity. By taking this approach, we can include the static friction phenomena in (2), without using (4). In this paper, we use (2) as the general description of discontinuous models.

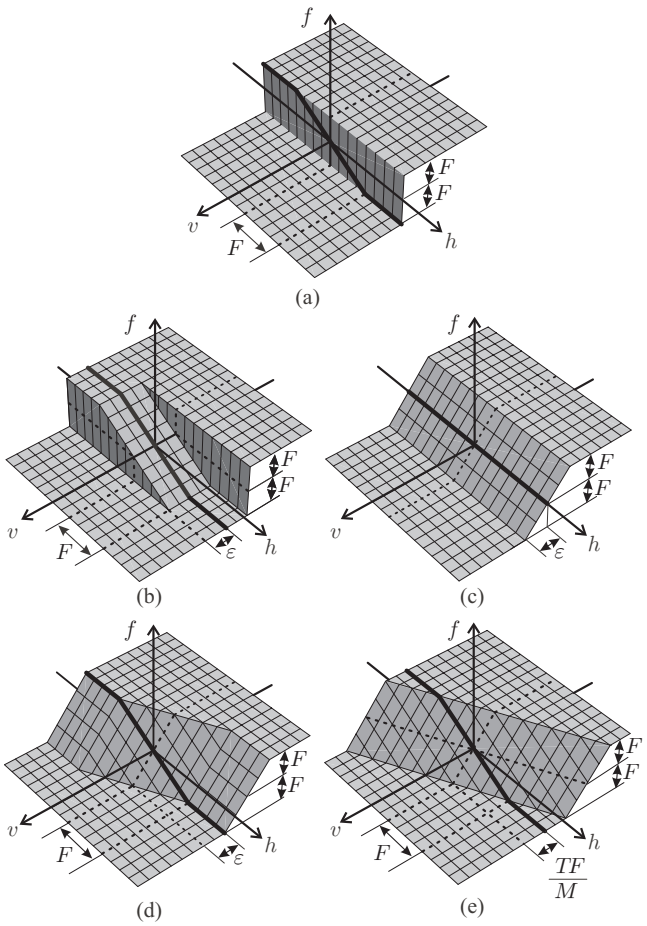

Fig. 3. Discontinuous friction models: (a) Coulomb friction model. (b) Karnopp's model [7], defined by (5) and (3), (c) viscosity approximation [14], defined by (6), (d) Quinn's model [8], defined by (7), and (e) the proposed discontinuous model, defined by (13). The thick black lines represent the value of f at $v = 0$. As $\varepsilon \to 0$ or $T \to 0$, (b), (d), and (e) converge to (a).

B. Discrete-Time Discontinuous Models

Difficulty in using the discontinuous friction models in digital computation is rooted in the definition of $\Phi(v, h)$ (defined in (2)) at $v = 0$. Fig. 3(a) shows the function $\Phi(v, h)$ in the case of Coulomb friction (3). Function $\Phi(v, h)$ is discontinuous with respect to v at $v = 0$, and $\Phi(v, h)$ depends on h exclusively when $v = 0$. Karnopp [7] avoided this problem by specifying a velocity region of a finite width as the zero-velocity region. This method can be described as follows:

$$f = \begin{cases} -h & \text{if } |v| \le \varepsilon \wedge |h| \le |\phi(\pm 0)| \\ -\mathrm{sgn}(h)|\phi(\pm 0)| & \text{if } |v| \le \varepsilon \wedge |h| > |\phi(\pm 0)| \\ \phi(v) & \text{otherwise,} \end{cases} \quad (5)$$

where ε is a small velocity below which the velocity is considered zero. This method has been widely used especially in the field of haptic display [12], [13]. However, it has been recognized that the behavior of the system is strongly dependent on the choice of the value ε [9]. Moreover, the threshold velocity cannot hold any physical meanings.

The plot of Karnopp's model, (5), is shown in Fig. 3(b). As

seen in this plot, $\Phi(v,h)$ is discontinuous at $v=\pm\varepsilon$. A method to remove this discontinuity is to approximate the friction force by a very high viscous friction force in the small velocity region [14]. This approach can be described as follows:

$$f=\begin{cases} -Fv/\varepsilon & \text{if } |v|\le\varepsilon \\ -\mathrm{sgn}(v)F & \text{otherwise.}\end{cases} \tag{6}$$

As illustrated in Fig. 3(c), this model is continuous but its behavior at $v=0$ is completely different from that of the Coulomb friction model. That is, the friction force does not balance the external force, h, at $v=0$.

In order to remove the discontinuities while maintaining consistency with the Coulomb friction model, Quinn [8] proposed the model equivalent to the following:

$$f=\begin{cases} -F\bar{v}/\varepsilon & \text{if } |\bar{v}|\le\varepsilon \\ -\mathrm{sgn}(\bar{v})F & \text{otherwise,}\end{cases} \tag{7a}$$

where

$$\bar{v}=\begin{cases} v+\varepsilon h/F & \text{if } |h|\le F \\ v+\mathrm{sgn}(h)\varepsilon & \text{otherwise.}\end{cases} \tag{7b}$$

This model is illustrated in Fig. 3(d). Its behavior is also influenced by the value ε, and unfortunately its optimal choice is not provided. Inclusion of arbitrary velocity-dependent friction (arbitrary $\phi(v)$) is not addressed in Quinn's paper.

In any methods mentioned above, the velocity does not reach zero in finite time even in the absence of external forces. This is an important difference from the continuous-time discontinuous friction models defined by (2). The velocity can be zeroed by using the detection of sign changes in the velocity [10], [11]. However, this approach is not suitable for multidimensional systems.

C. Continuous Models

Continuous friction models consider small elastic displacement (presliding displacement) in the sticking regime, as shown in Fig. 1(b). This elastic displacement is nonlinear and has hysteresis. The boundary between the sticking (presliding) regime and the sliding regime is usually ambiguous.

Most of modern continuous models have their roots in Dahl model [3]. Dahl model defines the friction force as

$$f=-Kz,\qquad \dot{z}=v\left(1-\mathrm{sgn}(v)Kz/F\right), \tag{8}$$

where z is a state variable that can be interpreted as the elastic displacement, and K correspondents to the initial stiffness coefficient in the presliding regime. The signs of v and f are chosen as Fig. 1(b). This model exhibits a continuous transition from the presliding regime to the sliding regime. Dahl model was unified with the Stribeck and viscous effects into the LuGre model [5]. One drawback of the Dahl and LuGre models is that they exhibit unbounded displacement under small forces. This drawback is eliminated from further improved models, the elastoplastic model [4], Leuven model [6], and the GMS (generalized Maxwell slip) model [15].

Modeling of hysteresis behavior in the presliding regime is also a matter of interest. The Maxwell slip model, which is illustrated in Fig. 4, is known to be effective for describing hysteresis behavior in mechanical systems [16]. This model is

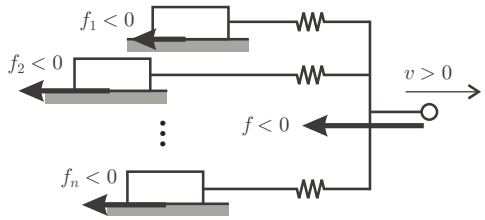

Fig. 4. The Maxwell slip model. Each element is massless and perfectly elastoplastic, having different friction forces.

the parallel connection of multiple ideal elastoplastic elements. A modified version of Leuven model [17] and the GMS model are based on the Maxwell slip model.

The GMS model is an extension of the Maxwell slip model to include arbitrary velocity-dependent friction forces. This model uses the following definition of the friction force:

$$f=-\textstyle\sum_{i=1}^{N}K_iz_i \tag{9a}$$

$$\dot{z}_i=\begin{cases} v & \text{if sticking} \\ \mathrm{sgn}(v)(\alpha_iQ/K_i)\left(1+K_iz_i/(\alpha_i\phi(v))\right) & \text{if sliding.}\end{cases} \tag{9b}$$

Here, Q is a constant and α_i is the fraction of the friction force exerted by the i-th element to the gross friction force, satisfying $\sum_{i=1}^{N}\alpha_i=1$. Equation (9b) is chosen so that f becomes equal to $\phi(v)$ when v is constant. Though (9b) is supported by simulation results of a more detailed physical model [18], there is no physical interpretation for this equation. A transition from the sliding regime to the sticking regime is triggered by the zero-crossing of the velocity v. Thus, this model is not easy to be used in multidimensional space.

III. New Discrete-Time Discontinuous Model

A. Simplest Case: Coulomb Friction

The friction force defined by (2) acts to make the object velocity reach zero in finite time. In this section, we propose a new discrete-time representation of (2) that guarantees convergence to zero-velocity in finite time and that does not contain arbitrariness of non-physical thresholds.

As shown in (1), the acceleration of the object is given by $\dot{v}=(h+f)/M$. Therefore, in a discrete-time system, the velocity at the next time step is determined as

$$v:=v+T\left(h+f\right)/M, \tag{10}$$

where T is the timestep size. The value of v in the left-hand side of (10) becomes zero if and only if

$$f=-h-Mv/T. \tag{11}$$

In the Coulomb friction model, defined by (2) and (3), the upper limit of the magnitude of f is F. Therefore, it is reasonable to define f as follows:

$$f=\begin{cases} -h-Mv/T & \text{if } |-h-Mv/T|\le F \\ \mathrm{sgn}\left(-h-Mv/T\right)F & \text{otherwise.}\end{cases} \tag{12}$$

The above definition can be rewritten as follows:

$$f=\begin{cases} -M\bar{v}/T & \text{if } |\bar{v}|\le TF/M \\ -\mathrm{sgn}(\bar{v})F & \text{otherwise,}\end{cases} \tag{13a}$$

where

$$\bar{v} = v + Th/M. \tag{13b}$$

This new model sets the velocity to be zero when $|h + Mv/T| \leq F$ is satisfied, and includes no arbitrariness such as threshold settings. A plot of (13) is shown in Fig. 3(e). This model is identical to the Coulomb friction model at $v = 0$, and is simpler than Quinn's and Karnopp's models. Moreover, it is interesting that the model (13) also reduces to the Coulomb friction model as $T \to 0$.

Let us use subscripts to denote time indices. Then, by using (10) and (13), we can determine v_k and f_k, the velocity and the friction force at time kT, respectively, as follows:

$$\bar{v} = v_{k-1} + Th_k/M \tag{14a}$$

$$f_k = \begin{cases} -M\bar{v}/T & \text{if } |\bar{v}| \leq TF/M \\ -\mathrm{sgn}(\bar{v})F & \text{otherwise} \end{cases} \tag{14b}$$

$$v_k = \bar{v} + Tf_k/M. \tag{14c}$$

B. Discrete-Time Discontinuous Model with Arbitrary Velocity-Dependent Friction

Due to the simplicity of (14b), it can easily be generalized to include arbitrary velocity-dependent friction laws. In (14b), note that $\mathrm{sgn}(\bar{v})$ is equal to $\mathrm{sgn}(v_k)$ because it is used under the condition $|\bar{v}| > TF/M$. Therefore, we can see that v_k and f_k satisfy the relation $f_k = \phi(v_k)$ when $\phi(\cdot)$ is defined by (3). This is an important difference of our model from both Karnopp's and Quinn's models, in which $f_k \approx \phi(v_{k-1})$ is intended to be satisfied.

Bearing this difference in mind, a natural generalization of (14b) can be written as follows:

$$f_k = \begin{cases} -M\bar{v}/T & \text{if } |\bar{v}| \leq T|\phi(\pm 0)|/M \\ \phi(v_k) & \text{otherwise.} \end{cases} \tag{15}$$

Unfortunately, because of (14c) and (15), v_k and f_k are mutually dependent and f_k is written as an implicit function of $\bar{v}$. This cyclic dependency can be removed by rewriting (15) as $f_k = \Phi^*(\bar{v})$ where

$$\Phi^*(a) = \begin{cases} -Ma/T & \text{if } |a| \leq T|\phi(\pm 0)|/M \\ \phi^*(a) & \text{otherwise} \end{cases} \tag{16a}$$

$$\phi^*(a) = f \quad \text{s.t.} \quad f = \phi\left(a + Tf/M\right). \tag{16b}$$

Namely, we now have a generalization of (14) as follows:

$$\bar{v} = v_{k-1} + Th_k/M \tag{17a}$$

$$f_k = \Phi^*(\bar{v}) \tag{17b}$$

$$v_k = \bar{v} + Tf_k/M. \tag{17c}$$

Fig. 5 illustrates the relation between $\phi(\cdot)$ and $\Phi^*(\cdot)$. In order to avoid solving the nonlinear algebraic equation (16b), we can practically assume

$$\phi^*(v) \approx \phi\left(v - \mathrm{sgn}(v)T|\phi(\pm 0)|/M\right) \tag{18}$$

if $\phi(v)$ is sufficiently smooth in $v > 0$ and $v < 0$.

In (17), $\bar{v}$ can be interpreted as the velocity that could have been achieved if no friction force acted. It is straightforward to see that $|v_k| < |\bar{v}|$ if $|\bar{v}| > 0$, and that $v_k = 0$ if $\bar{v} = 0$. This means that, in (17), the friction force, f_k, always acts to decrease the kinetic energy. That is, this friction model is guaranteed to be dissipative with any T.

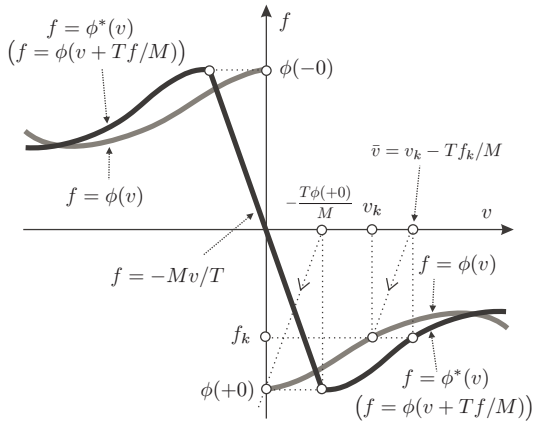

Fig. 5. Definition of $\Phi^*(v)$ to guarantee $f_k = \phi(v_k)$. The black curve represents $f = \Phi^*(v)$.

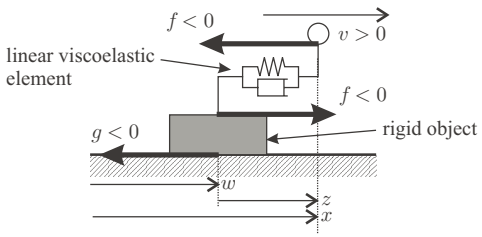

Fig. 6. A linear continuous model. The input is v, and the output is f.

Equations (16) and (17) can be generalized to multidimensional cases because they are still valid even if v, $\bar{v}$, h, and f are vectors. Especially in the case of Coulomb friction, we can simply use (14) by interpreting $\mathrm{sgn}(\cdot)$ as the normalization function $\mathrm{sgn}(a) = a/|a|$. One difficulty is that the algebraic equation (16b) is sometimes difficult to be solved. Adequate approximations for (16b) need to be sought. Also, if M is a matrix, not a scalar, (16) and (17) will need further modifications. This remains for future study.

The dependence on the knowledge of M may be seen as a drawback of the proposed method. However, M is always known as long as it is a virtual mass set in the simulator. If M is a real mass, it has to be given in advance. The model's sensitivity to the error in M should be clarified in continuing study.

IV. New Discrete-time Continuous Model

A. Linear Continuous Model

Next, we consider to utilize the proposed discontinuous model of section III-B to construct a continuous model of friction. A serial connection of the discontinuous model and a linear viscoelastic element, which is shown in Fig. 6, is the simplest example of a continuous model. Let x and v denote the position and velocity of the end-point of the viscoelastic element, respectively. Let w denote the position of the mobile object. Let f and g denote the reaction force

from the viscoelastic element and the force applied to the mobile object by the fixed surface, respectively. The input to this system is v or x, and the output from the system is f. The variable w is the state variable of this system. In haptic rendering, x corresponds to the position of the haptic device, and f corresponds to the force to be generated by the haptic device.

The force f, which is determined by the viscoelastic element, can be written as follows:

$$f = -K(x - w) - B(\dot{x} - \dot{w}). \tag{19}$$

where K and B are the stiffness and viscosity of the viscoelastic element. These parameters determine the model's behavior in the presliding regime. The equation of motion of the mobile object is:

$$M\ddot{w} = g - f. \tag{20}$$

Here, g is determined as $g = \Phi(\dot{w}, -f)$, depending on the relative velocity, $\dot{w}$, and the external force, $-f$. The discrete-time representation of (20) is

$$\Delta w_k = \Delta w_{k-1} + T^2(g_k - f_k)/M, \tag{21}$$

where $\Delta w_k = w_k - w_{k-1}$.

By directly using the method in section III-B, we can write a discrete-time representation of this system as follows:

$$f_k = -K(x_k - w_{k-1}) - B\left(\Delta x_k - \Delta w_{k-1}\right)/T \tag{22a}$$
$$\bar{v} = \Delta w_{k-1}/T - Tf_k/M \tag{22b}$$
$$g_k = \Phi^*(\bar{v}) \tag{22c}$$
$$\Delta w_k = T\bar{v} + T^2 g_k/M, \tag{22d}$$

where $\Phi^*(\cdot)$ is that defined by (16a) and $\Delta x_k = x_k - x_{k-1}$. This representation is straightforward to understand. However, it cannot be used if $M = 0$ because of the divisions by M.

In stead of using (22a), we here consider to use the following definition of f_k:

$$\begin{aligned} f_k &= -K(x_k - w_k) - B\left(\Delta x_k - \Delta w_k\right)/T \\ &= -K(x_k - w_{k-1}) - B\Delta x_k/T + (K + B/T)\Delta w_k. \end{aligned} \tag{23}$$

Notice that w is one step ahead of that in (22a). In other words, (23) is based on the backward difference scheme, while (22a) is based on the forward difference scheme. Because of (21) and (23), Δw_k and f_k are mutually dependent. Algebraically solving (21) and (23) yields

$$\Delta w_k = T\bar{u} + T^2 g_k/C, \tag{24}$$

where

$$\bar{u} = \frac{\Delta x_k}{T} + \frac{TK}{C}(x_{k-1} - w_{k-1}) - \frac{M(\Delta x_k - \Delta w_{k-1})}{TC} \tag{25}$$
$$C = M + TB + T^2K. \tag{26}$$

There is a similarity between (17c) and (24). When $\Delta w_k \neq 0$, the force g_k is determined by the relative velocity, i.e., $g_k = \phi(\Delta w_k/T)$. On the other hand, substituting (24) by $\Delta w_k = 0$ yields $g_k = -C\bar{u}/T$, and this can hold only if $|g_k| \leq |\phi(\pm 0)|$. Therefore, in the same manner as we wrote (15), we can write

$$g_k = \begin{cases} -C\bar{u}/T & \text{if } |\bar{u}| \leq T|\phi(\pm 0)|/C \\ \phi(\Delta w_k/T) & \text{otherwise.} \end{cases} \tag{27}$$

In the same manner as we replaced (15) by (17b), we can replace (27) by $g_k = \Phi^c(\bar{u})$ where

$$\Phi^c(a) = \begin{cases} -Ca/T & \text{if } |a| \leq T|\phi(\pm 0)|/C \\ \phi^c(a) & \text{otherwise,} \end{cases} \tag{28a}$$
$$\phi^c(a) = f \quad \text{s.t.} \quad f = \phi\left(a + Tf/C\right). \tag{28b}$$

By using this, we can write another discrete-time representation of this system as follows:

$$\bar{u} = v_k + \frac{TK}{C}z_{k-1} - \frac{M}{C}\left(v_k - v_{k-1} + \frac{\Delta z_{k-1}}{T}\right) \tag{29a}$$
$$g_k = \Phi^c(\bar{u}) \tag{29b}$$
$$\Delta z_k = Tv_k - T\left(\bar{u} + Tg_k/C\right) \tag{29c}$$
$$f_k = -Kz_k - B\Delta z_k/T, \tag{29d}$$

where $v_k = \Delta x_k/T$, $z = x - w$, and $z_k = z_{k-1} + \Delta z_k$.

Unlike the system (22), the system (29) can be used even if $M = 0$. If we set $M = 0$, $B = 0$, and $\phi(v) = -\mathrm{sgn}(v)F$, this system reduces to a perfect elastoplastic, massless element, and becomes equivalent to a model presented by Hayward and Armstrong [19].

B. Compound Continuous Model with Presliding Hysteresis

The linear continuous model of section IV-A exhibits a linear viscoelastic behavior in the presliding regime. Inclusion of hysteresis in this model is not straightforward. However, recall that the Maxwell-slip model, which exhibits a hysteresis behavior, is a parallel connection of multiple perfect elastoplastic, massless elements. The linear continuous model of section IV-A is a viscoelasto-plastic element that allows nonzero mass and velocity-dependent friction forces. Therefore, a parallel compound of multiple instances of the linear continuous model is a generalization of the Maxwell-slip model.

Lampaert et al.'s GMS model [15] is also a generalization of the Maxwell-slip model. As we pointed out in section II-C, the GMS model has difficulties in its physical interpretation and extensibility to multidimensional cases. On the contrary, our compound continuous model is physically intuitive and extensible to multidimensional cases. One of its weakness is that it does not include the frictional lag, which is a time lag between the velocity and the velocity-dependent friction [2]. This phenomenon, however, is peculiar to lubricated friction, and may be included by considering the dynamics of lubricants. Nevertheless, this model needs some improvements and validations to be an accurate model of real frictional phenomena.

At this point, we can mention that the compound continuous model can be useful for haptic rendering of friction. When the linear continuous model is used, transitions from the presliding regime to the sliding regime are instantaneous, and this can cause somewhat unnatural sensations. To the contrary, the compound continuous model with hysteresis can generates

TABLE I

FRICTION MODELS USED IN SIMULATIONS I AND II

K1	:	Karnopp's model with $\varepsilon = 1$ m/sec
K2	:	Karnopp's model with $\varepsilon = 0.01$ m/sec
K3	:	Karnopp's model with $\varepsilon = 0.0001$ m/sec
Q1	:	Quinn's model with $\varepsilon = 1$ m/sec
Q2	:	Quinn's model with $\varepsilon = 0.01$ m/sec
Q3	:	Quinn's model with $\varepsilon = 0.0001$ m/sec
P	:	Proposed discontinuous model

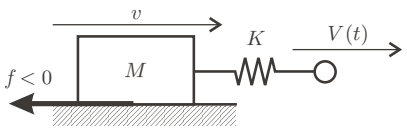

Fig. 7. Simulation I.

smooth, continuous transitions, causing a natural feeling of a frictional surface. Psychophysical experiments to validate the usefulness are subject to continuing work.

V. NUMERICAL SIMULATIONS

A. Simulation I: Comparison of the Proposed Discontinuous Model with Karnopp's and Quinn's models

The proposed discontinuous model was compared to Karnopp's and Quinn's models in numerical simulations. As illustrated in Fig. 7, an object with a mass of $M = 1$ kg was attached to a spring with stiffness 90 N/m, and the end of the spring was moved with a time-varying velocity $V(t)$, which was 2 m/sec before $t = 2$ sec, and zero otherwise. A Coulomb friction force of $F = 10$ N acted on the object. The timestep size was 0.001 sec.

Table I lists seven models used in the simulation. Three are Karnopp's models with different ε values, another three are Quinn's models with different ε values, and the last one is the proposed model. With each of the seven models, the velocity, v, and the friction force, f, are shown in Fig. 8. The gray lines in the velocity graph represent the plots of $V(t)$.

The result of Model K1 is clearly inappropriate. Model Q1, which has a large ε, asymptotically approaches zero velocity, but is too slow in convergence. Models K3 and Q3, which have a very small ε, show oscillation in the force at and after the stop ($t \geq 2$ sec). Model K2 maintains a positive nonzero velocity even after $t = 3$, which causes a change in the spring force to the negative direction, and consequently the friction force changes to the positive direction.

Results of Models Q2 and P are almost identical to each other. This is because Quinn's model with $\varepsilon = TF/M$ and the proposed model are identical in the region $|h| \leq F$, as illustrated in Fig. 3. These results do not demonstrate the advantage of Model P over Model Q2. However, it should be noted that this is because $\varepsilon = 0.01$ m/sec is the optimal value for Quinn's model in this case.

B. Simulation II: Comparison of the Proposed Discontinuous Model with Optimized Quinn's model

By comparing Fig. 3(d) and (e), one can see that the proposed discontinuous model (Model P) and the optimized

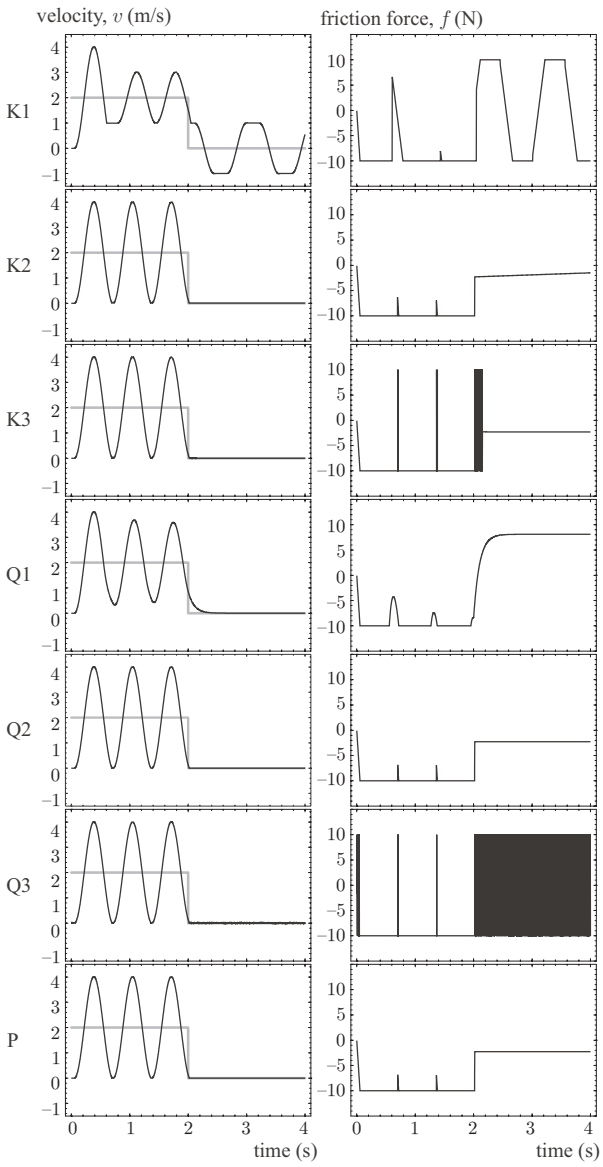

Fig. 8. Results of Simulation I: Comparison of discontinuous friction models.

Quinn's model (Model Q2) are different only in the region where the external force is larger than the friction force ($|h| > F$) and the velocity is close to zero. In order to exhibit this difference, we performed another simulation. A mobile object with a mass of $M = 1$ kg was used. The object was given an initial velocity of $v = -0.13$ m/sec, and was pulled to the positive direction with the force of 40 N. The friction force was $F = 10$ N, and the timestep size was 0.001 sec.

The results are shown in Fig. 9. The gray lines represent analytical values (accurate values obtained by the continuous time representation). Notice that the scales of time and velocity are very different from that of Fig. 8. As shown in Fig. 9, Models P and Q2 exhibit different behaviors at the instant of zero-velocity crossing. After the zero-velocity crossing ($t \geq 0.004$ sec), the velocity of Model Q2 is larger than the analytical value. This is because, at the time of zero-velocity

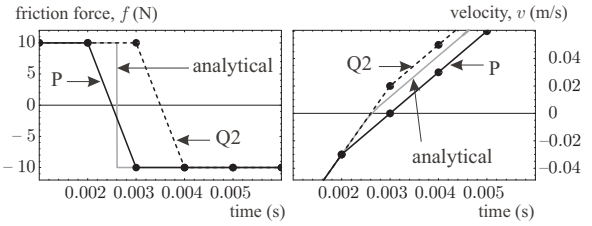

Fig. 9. Results of Simulation II: Comparison of models P with Q2. The external force is constant. Gray lines represent analytical results.

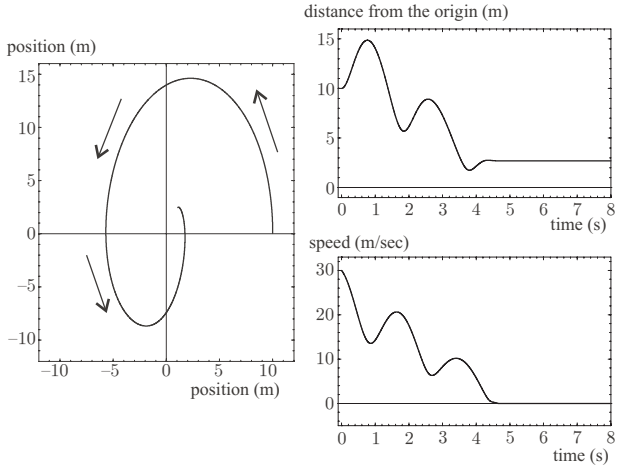

Fig. 10. Results of Simulation III: A two-dimensional discontinuous model.

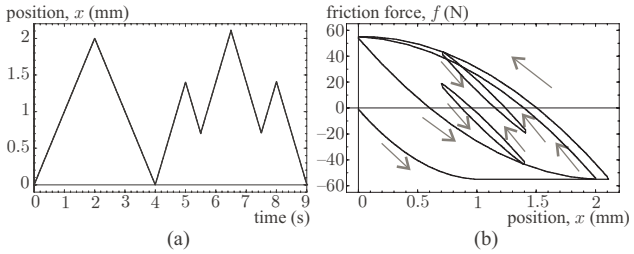

Fig. 11. Simulation IV: A compound continuous model. (a) The position signal. (b) The resultant friction force as the function of position.

crossing ($t = 0.003$ sec), the friction force of Model Q2 acted to increase the kinetic energy. On the other hand, the friction force of Model P always decreases the kinetic energy. Therefore, the proposed discontinuous model is a slightly overdissipative approximation of the analytical model. A slightly overdissipative approximation is preferable to energy-generating approximations especially in haptic rendering.

The difference demonstrated here may be criticized as too small. However, we emphasize that our model has no arbitrariness in the parameter setting, while Quinn's model has to be tuned so that it can behave in a stable, realistic manner.

C. Simulation III: Two-Dimensional Friction

Another simulation was performed to validate the discontinuous model in multidimensional space. An object ($M = 1$ kg) was placed on a frictional surface. It was connected to a spring (spring constant 3 N/m, natural length 0 m) whose other end was fixed at the origin. At $t = 0$ sec, the object was placed at the position of $(10, 0)$ m, and was given the initial velocity of $(0, 30)$ m/sec. The friction force of $F = 10$ N acted in the opposite direction of the velocity, and the spring force acted to pull the object to the origin. Fig. 10 shows the results. The object completely stops at $t = 4.5$ sec with no vibratory behaviors.

D. Simulation IV: Hysteresis Behavior

The compound continuous model of section IV-B was also tested by a simulation. Ten instances of the linear continuous model with $K = 10$ N/mm, $B = 0.1$ Ns/mm, $M = 0$ kg, and $F = 1, 2, \cdots, 10$ N were connected in parallel. The position signal shown in Fig. 11(a) was provided to the system, and the resultant force was recorded. The timestep size was 0.001 sec. Fig. 11(b) shows the resultant position-force plot. This shows that this model exhibits a smooth hysteresis behavior. All loops are closed. This is an important characteristic of the hysteresis in real mechanical systems.

VI. Experiment: Haptic Rendering of Planar Friction

We performed a preliminary experiment using the 2-DOF parallel link manipulator shown in Fig. 12. We used this manipulator as a haptic device. AC servomotors with Harmonic drive gearings were mounted on the joints. A 6-axis force sensor (Nitta IFS) was attached to the end of the manipulator. The experimenter grasped and moved the grip attached to the force sensor. This manipulator has large friction in its joints (approximately 10 Nm).

We used the discontinuous model of two-dimensional version. In this model, the mass of the (virtual) object was 2 kg, and the magnitude of Coulomb friction force was 6 N. The timestep size (sampling interval) was 0.001 sec. The force measured by the force sensor was provided to the model, and the friction force was calculated. The position of the virtual object was updated according to these forces. The position of the manipulator was controlled to follow the position of the virtual object by using PD controllers on the joint angles.

Fig. 13 shows the results. The thick curve represents the position trajectory of the end-effector, and the thin line segments represent the force measured by the force sensor every 0.02 sec, which are the forces applied by the experimenter. In the region from **a** through **d**, the force is in the same direction of the motion because the trajectory is straight. At the point **c**, the force from the experimenter's hand is lower than the friction force, and thus the end-effector is stationary. In the region from **d** to **e**, the experimenter's force resists the friction force and the centrifugal force. Thus, the vectors are slanted to the inside of the curve.

One might assume that the forces in Fig. 13 may be attributed to the friction in the manipulator joints. However, the end-effector forces caused by the joint friction would be anisotropic and dependent on the manipulator configuration, while the forces in Fig. 13 are isotropic and homogeneous. The joint friction torques are almost totally annihilated by the stiff PD position controllers.

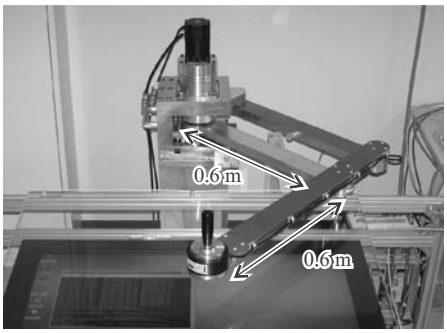

Fig. 12. Experimental setup.

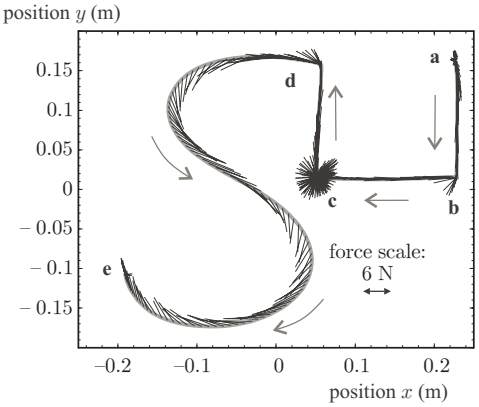

Fig. 13. Experimental results. The thick curve represents the position trajectory. The thin line segments represent the force measured by the force sensor.

Because of the large friction in the joints, there are some difficulties in using the continuous model with this manipulator. The continuous model, which requires a velocity input, will be effectively implemented in low-friction, low-inertia haptic devices, such as PHANToM interfaces.

VII. Conclusion

We have presented two discrete-time models of friction for the purpose of fixed-step numerical simulations. The first one is a Coulomb-like discontinuous model. This model determines the friction force so that the velocity reaches zero in finite time. The second one is a serial connection of a discontinuous friction model and a linear viscoelastic element. These models are numerically robust and easily extended into multidimensional cases. They can include arbitrary velocity-dependent friction forces. The second model can be extended into a more sophisticated friction model, which exhibits a hysteresis behavior in the presliding regime. Results of numerical simulations and an experiment have been presented.

The presented models will be useful for haptic rendering of friction. Another potential application is the use as a friction compensator in control systems. Some improvements regarding modeling of lubricant behaviors are topics of future research. The influence of the errors and noises in velocity measurement also remains to be investigated.

We intend to apply the presented technique to power-assist devices for conveying heavy components in the automobile industry [20]. Coulomb friction forces implemented by the presented technique will be suitable for accurate positioning [12].

This work has been supported by Toyota Motor Corporation. We thank the engineers of Toyota Motor Corporation who motivated and inspired our research.

References

[1] B. Armstrong-Hélouvry, P. Dupont, and C. Canudas de Wit, "A survey of models, analysis tools and compensation methods for the control of machines with friction," *Automatica*, vol. 30, no. 7, pp. 1083–1138, 1994.

[2] H. Olsson, K. J. Åström, C. Canudas de Wit, M. Gäfvert, and P. Lischinsky, "Friction models and friction compensation," *European J. of Control*, vol. 4, pp. 176–195, 1998.

[3] P. R. Dahl, "A solid friction model," Aerospace Corporation, Tech. Rep. TOR-0158(3107-18)-1, 1968.

[4] P. Dupont, V. Hayward, B. Armstrong, and F. Altpeter, "Single state elastoplastic friction models," *IEEE Trans. on Automatic Control*, vol. 47, no. 5, pp. 787–792, 2002.

[5] C. Canudas de Wit, H. Olsson, K. J. Åström, and P. Lischinsky, "A new model for control of systems with friction," *IEEE Trans. on Automatic Control*, vol. 40, no. 3, 1995.

[6] J. Swevers, F. Al-Bender, C. G. Ganseman, and T. Prajogo, "An integrated friction model structure with improved presliding behavior for accurate friction compensation," *IEEE Trans. on Automatic Control*, vol. 45, no. 4, pp. 675–686, 2000.

[7] D. Karnopp, "Computer simulation of stick-slip friction in mechanical dynamic systems," *Trans. of ASME: J. of Dynamic Systems, Measurement, and Control*, vol. 107, no. 1, pp. 100–103, 1985.

[8] D. D. Quinn, "A new regularization of Coulomb friction," *Trans. of ASME: J. of Vibration and Acoustics*, vol. 126, no. 3, pp. 391–397, 2004.

[9] C. Richard, "On the identification and haptic display of friction," Ph.D. dissertation, Stanford University, 2000.

[10] A. Bonsignore, G. Ferretti, and G. Magnani, "Analytical formulation of the classical friction model for motion analysis and simulation," *Mathematical and Computer Modelling of Dynamical Systems*, vol. 5, no. 1, pp. 43–54, 1999.

[11] F. A. Tariku and R. J. Rogers, "Improved dynamic friction models for simulation of one-dimensional and two-dimensional stick-slip motion," *Trans. of ASME: J. of Tribology*, vol. 123, no. 4, pp. 661–669, 2001.

[12] C. Richard and M. R. Cutkosky, "Friction modeling and display in haptic applications involving user performance," in *Proc. of the 2002 IEEE Int. Conf. on Robotics and Automation*, 2002, pp. 605–611.

[13] S. E. Salcudean and T. Vlaar, "On the emulation of stiff walls and static friction with a magnetically levitated input-output device," *Trans. of ASME: J. of Dynamic Systems, Measurement, and Control*, vol. 119, pp. 127–132, 1997.

[14] J. A. C. Martins and J. T. Oden, "A numerical analysis of a class of problems in elastodynamics with friction," *Computer Methods in Applied Mechanics and Engineering*, vol. 40, no. 3, pp. 327–360, 1983.

[15] V. Lampaert, J. Swevers, and F. Al-Bender, "A generalized Maxwell-slip friction model appropriate for control purposes," in *Proc. of the 2003 Int. Conf. on Physics and Control*, pp. 1170–1177.

[16] W. D. Iwan, "A distributed-element model for hysteresis and its steady-state dynamic response," *Trans. of ASME: J. of Applied Mechanics*, vol. 33, no. 4, pp. 893–900, 1966.

[17] V. Lampaert, J. Swevers, and F. Al-Bender, "Modification of the Leuven integrated friction model structure," *IEEE Trans. on Automatic Control*, vol. 47, no. 4, pp. 683–687, 2002.

[18] F. Al-Bender, V. Lampaert, and J. Swevers, "A novel generic model at asperity level for dry friction force dynamics," *Tribology Letters*, vol. 16, no. 1, pp. 81–93, 2004.

[19] V. Hayward and B. Armstrong, "A new computational model of friction applied to haptic rendering," in *Experimental Robotics VI*, P. Corke and J. Trevelyan, Eds. Springer, 2000, pp. 404–412.

[20] Y. Yamada, H. Konosu, T. Morizono, and Y. Umetani, "Proposal of skill-assist: A system of assisting human workers by reflecting their skills in positioning tasks," in *Proc. of the 1999 IEEE Int. Conf. on Systems, Man, and Cybernetics*, vol. 4, 1999, pp. 11–16.